Eur. Phys. J. B **35**, 133–141 (2003)
DOI: 10.1140/epjb/e2003-00264-6

THE EUROPEAN PHYSICAL JOURNAL B

Turbulent thermal convection in a closed domain: viscous boundary layer and mean flow effects

R. Verzicco[a]

Politecnico di Bari, DIMeG and CEMeC, Via Re David 200, 70125, Bari, Italia

Received 7 March 2003
Published online 22 September 2003 – © EDP Sciences, Società Italiana di Fisica, Springer-Verlag 2003

Abstract. In this paper the effects of viscous boundary layers and mean flow structures on the heat transfer of a flow in a slender cylindrical cell are analysed using the direct numerical simulation of the Navier–Stokes equations with the Boussinesq approximation. Ideal flows are produced by suppressing the viscous boundary layers and by artificially enforcing the flow axisymmetry with the aim of checking some proposed explanations for the Nusselt number dependence on the Rayleigh number. The emerging picture suggests that, in this slender geometry,the presence of the viscous boundary layers does not have appreciable impact on the slope of the Nu *vs.* Ra relation while a transition of the mean flow is most likely the reason for the slope increase observed around $Ra = 2 \times 10^{9}$.

PACS. 47.27.Te Convection turbulent flows – 47.32.-y Fluid flow buoyant – 44.25.+f Heat transfer convective

1 Introduction

One of the main advantages of numerical simulation is the possibility to perform ideal experiments with the aim of verifying conjectures or stressing the hypotheses of a theory. Indeed, in thermal convection a numerical simulation is always an ideal experiment owing to the precise assignment of the temperature boundary conditions, the possibility of having plates with infinite heat capacity, the absence of conductive side–wall effects and the unconditional validity of the Boussinesq approximation that in laboratory experiments might be cause of concern ([1–5]). Nevertheless, in this context, by ideal experiments we mean flows that can not be realized, even in an approximate way, by a real experimental apparatus. In particular we will consider the flow developing in a cylindrical cell of aspect ratio (diameter over height) $\Gamma = 1/2$ heated from below and cooled from above with an adiabatic side wall and with free–slip boundaries, thus preventing the formation of viscous boundary layers. The results will be then compared with previous and new simulations with the same temperature boundary conditions but with ordinary no–slip walls. Another ideal experiment consists of simulations in which the flow is forced to remain axisymmetric; this strongly alters the structure of the mean flow with respect to the full three–dimensional configuration thus allowing the analysis of the effect of coherent large scales on the heat transfer.

The motivation for this study comes from several papers in which the roles of mean flow and viscous boundary layers (and the kinetic energy therein dissipated) are considered for the heat transfer as function of the maximum temperature difference in the system. These parameters are expressed in non dimensional form by the Nusselt Nu and Rayleigh Ra numbers (see next section for the definitions) which can be considered, respectively, as response and input of the system. The seminal paper by Castaing *et al.* [6] showed the 2/7 power law in the Nu *vs.* Ra relation for gaseous helium and, even if it is now clear that a simple power law does not fit the whole curve, several theories have been proposed for the explanation of the scaling. Shraiman and Siggia [7], for example, were able to derive the correct power law by assuming a thermal boundary layer contained within the viscous one and a linear velocity profile induced by the latter; it can be shown that this is equivalent to assume that the most of the kinetic energy dissipation of the system occurs in the viscous boundary layers.

The scenario was complicated by recent experiments in gaseous helium ([3,8–10]) in which the Nu *vs.* Ra relation showed a transition above $Ra \simeq 10^{11}$ toward a steeper power law, perhaps indicating the occurrence of the Kraichnan [11] asymptotic regime $Nu \sim Ra^{1/2}$. Apparently, all this complex dynamics is unified under the theory by Grossmann and Lohse [12,13] which classifies the flows in the Ra–Pr phase space according to the dominant contribution (bulk or boundary layer) to the kinetic energy and temperature variance dissipation rates; the theory is also successful in predicting the Nu *vs.* Pr dependence and the Reynolds number variation with Ra and Pr (Pr is the Prandtl number defined in the next

[a] e-mail: verzicco@poliba.it

section). The recent paper by Verzicco and Camussi [14] has however shown that in a cylindrical cell of aspect ratio $\Gamma = 1/2$ at $Pr = 0.7$ and $2 \times 10^6 \leq Ra \leq 2 \times 10^{11}$ the direct computation of the boundary layers thickness and their contribution to the total dissipation rates yields a picture which does not agree with that given by the Grossmann and Lohse [13] phase diagram. It was then shown that in the slender geometry the mean flow behaved in a peculiar way and it was conjectured that that could be the cause for the disagreement with the theory.

The purpose of this study is to investigate in more detail the above points and, in particular, the role of the viscous boundary layers and of the mean flow on the Nu *vs.* Ra relation.

2 Numerical set–up

The flow investigated in this paper is that developing in a cylindrical cell of aspect ratio $\Gamma = 1/2$ heated from below and cooled from above with an adiabatic side wall. All the cell surfaces are no–slip; in a set of numerical experiments, however, free–slip boundary conditions have been imposed in order to prevent the formation of viscous boundary layers and to investigate their effects on the flow dynamics. The former configuration (with the no–slip boundaries) replicates the set–up of recent studies ([9,14–17]) that performed experiments and numerical simulations using gaseous helium close to the critical point as working fluid. For this problem the controlling parameters are $Ra = g\alpha\Delta h^3/(\nu k)$ and $Pr = \nu/k$ where Δ and h denote the temperature difference between the plates and their separation distance, respectively, and g is the acceleration of gravity. The fluid properties are retrieved by the parameters α, ν and k which are, respectively, the thermal expansion coefficient, the kinematic viscosity and the thermal diffusivity. The heat transfer between the plates is expressed in nondimensional form by $Nu = Qh/(\lambda\Delta)$ with Q the heat per unit surface transferred between the two plates and λ the thermal conductivity. The flow is solved by numerically integrating the three–dimensional unsteady Navier–Stokes equations with the Boussinesq approximation. The equations have been written in a cylindrical coordinate frame and discretized on a staggered mesh by central second–order accurate finite–difference approximations; the resulting discretized system is solved by a fractional–step procedure with the elliptic equation inverted using trigonometric expansions in the azimuthal direction and a direct solver for the other two directions. The time advancement of the solution is obtained by a hybrid low–storage third–order Runge–Kutta scheme. The numerical method is the same as that described in [14] (hereafter referred to as VC03) where further details of the numerical procedure can be found.

Thanks to the data accessibility provided by the direct numerical simulation three–dimensional velocity and temperature fields have been employed for the computation of kinetic energy and temperature variance dissipation rates $\epsilon = \sqrt{Pr/Ra}\langle|\nabla\mathbf{u}|^2\rangle$ and $N = 1/\sqrt{RaPr}\langle|\nabla\theta|^2\rangle$ through

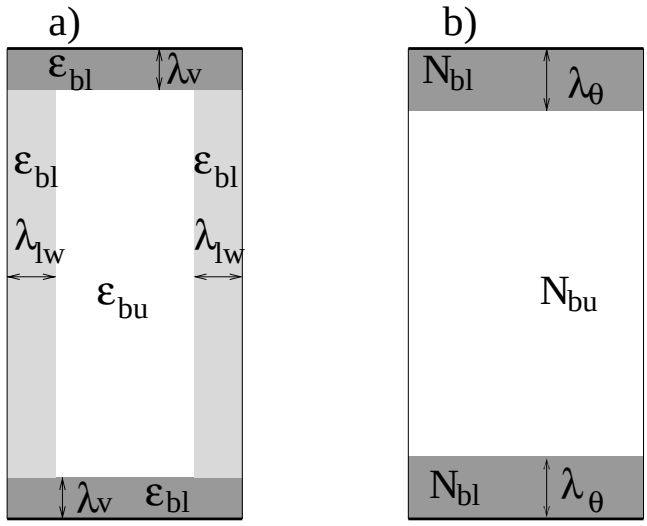

Fig. 1. Sketch of the boundary layer/bulk region separation for kinetic energy dissipation rate ϵ (a)) and temperature variance dissipation rate N (b)).

the spatial gradients of velocity $\mathbf{u}$ and temperature θ. As suggested by Grossmann and Lohse [12], for the analysis of the results it will be useful to separate the contributions to ϵ and N coming from boundary layer (ϵ_{bl}, N_{bl}) and bulk (ϵ_{bu}, N_{bu}) flow regions; in order to avoid confusion in Figure 1 a sketch is given showing the different regions. λ_v and λ_{lw} are, respectively, the viscous boundary layer thicknesses on the plates and on the side wall (the former being thinner than the latter) while λ_θ is the thickness of the thermal boundary layer on the plates. It is worth noting that being the lateral wall thermally adiabatic and no–slip it will contribute to ϵ_{bl} and not to N_{bl} which, instead, is generated only in the plate region.

The reference data consist of 6 simulations at $Pr = 0.7$ and Ra in the range $2 \times 10^6 - 2 \times 10^{11}$ reported in VC03; those simulations have been validated with laboratory experiments and verified by grid refinements checks. We have used therefore those data as benchmarks to assess the quality of the present new simulations. Three sets of numerical experiments have been run: in the first the Prandtl number was increased to $Pr = 4$ to mimic the behaviour of water at $T = 45$ °C and the Rayleigh number was varied in the range $2 \times 10^6 \leq Ra \leq 2 \times 10^{10}$. The second set is identical to the first but for the velocity boundary conditions which are free–slip on all the cell surfaces. This prevents the formation of viscous boundary layers and their influence on the flow dynamics can be studied. The last set of experiments consists of axisymmetric simulations at $Pr = 4$ the Rayleigh number in the range $2 \times 10^6 \leq Ra \leq 2 \times 10^{11}$ and ordinary no–slip velocity boundary conditions; these simulations allowed to investigate the effect of the mean flow structure, and in particular of the single recirculation completely filling the cell, on the heat transfer.

Using the results of VC03 it was verified that for every three–dimensional simulation the mesh size in the bulk was of the same order as the the Kolmogorov scale and

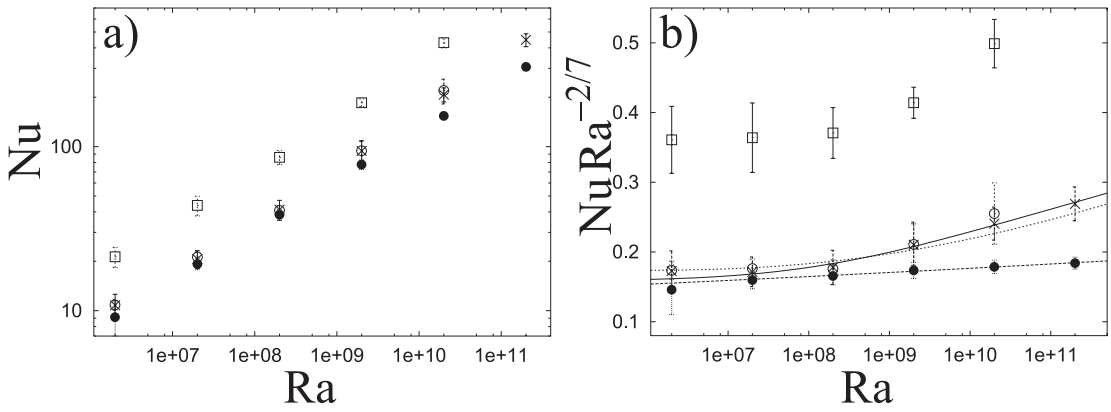

Fig. 2. a) Nusselt *vs.* Rayleigh: × $Pr = 0.7$ (data from VC03); ○ $Pr = 4$, □ $Pr = 4$ free–slip walls; • $Pr = 4$ axisymmetric flow. b) The same as a) for the compensated Nusselt number; – – – – $y = x^{0.015}$ power law ($Nu \sim Ra^{0.3}$), ——— fit of equation (1) at $Pr = 0.7$ ····· fit of equation (1) at $Pr = 4.0$.

that viscous and thermal boundary layers at the solid surfaces were adequately resolved (a minimum of 5 points inside the thermal layer with the first point within 1/8 of the layer thickness). This resulted in a non–uniform mesh in the radial and vertical directions with grids ranging from $65 \times 49 \times 129$ up to $129 \times 97 \times 385$, respectively, in the azimuthal radial and vertical directions. The simulation at $Pr = 4$ and $Ra = 2 \times 10^{10}$ with free–slip walls is the only exception to the mentioned resolution requirements; in fact we will see in Section 3.2 that the main effect of the viscous layer suppression is a decrease of the thermal boundary layer thickness by almost a factor 2. As a consequence we found that only three nodes were within the thermal boundary layer and, although this resolution is considered adequate by Grötzbach [18], we would regard the results of this simulation only as indicative rather than quantitatively reliable. In the set of axisymmetric simulations the Rayleigh number was increased up to $Ra = 2 \times 10^{11}$ and therefore the grid was refined to 129×513 points in the radial and vertical directions. An extra simulation was run with a more refined grid (193×769) to check the results of the previous run.

As a further check, following VC03, the Nusselt number was computed in two ways: $Nu = 1 + \sqrt{RaPr}\langle u_x \theta \rangle$, with the angular brackets indicating average over time and over the whole fluid layer, and $Nu = \overline{\partial\theta/\partial x}|_w$ where $|_w$ indicates that the derivative is evaluated at the wall and the overbar implies an average in time and over the plate surface. The two definitions converge to the same value provided the spatial resolution is adequate both in the bulk and in the wall region and that the evolution is long enough to average out the small mean temperature fluctuations (VC03).

All the simulations have been run for a long enough time to compute reliable statistics for the heat transfer and other second order moments (like r.m.s profiles of velocity and temperature); also in this case the estimates from VC03 have been used and these required a total simulation time T_{tot} from $100T_L$ to $165T_L$ (with $T_L = 2h/U$ the large–eddy–turnover time, and $U = \sqrt{g\alpha\Delta h}$ the free–fall velocity) for the Rayleigh number $2\times10^6 \leq Ra \leq 2\times10^{10}$.

3 Results

The main result which will drive the discussion of all the numerical experiments is that reported in Figure 2 showing the increase of the Nusselt number with the Rayleigh number for different flow conditions.

Several facts are evident from Figure 2: i) all the three dimensional flows show a change in the slope of the Nu *vs.* Ra curve which in VC03 was found to be due to a modification of the mean flow structure. ii) The experiments at $Pr = 0.7$ and $Pr = 4$ show the same values of the Nusselt number and the same location for the slope change thus implying that the present Prandtl number variation does not have any appreciable effect on the non dimensional heat transfer. iii) The flow with the free–slip boundary conditions, in contrast, has a heat transfer which is about twice bigger than that of the analogous flow with no–slip velocity boundary conditions; nevertheless both the power law dependence on Ra and the position of the slope change are the same. iv) Finally the axisymmetric flow has the smallest values of the Nusselt number and, in the explored range of Rayleigh numbers, is characterized by a constant slope which is to a good approximation $Nu \sim Ra^{0.3}$.

The successives sections will investigate the different flow features to justify the above observations.

3.1 Prandtl number effect

As anticipated by the results of Figure 2 the Nusselt number at $Pr = 0.7$ and $Pr = 4$ is essentially the same and this result agrees with those in [10] who experimentally studied the same flow in a range of Prandtl numbers $0.7 \leq Pr \leq 21$. The same independence of the Nusselt number on the Prandtl number was observed by Ahlers and Xu [19] in the range $4 \leq Pr \leq 34$; in particular

within one decade of Pr their variation of the Nusselt number was only about 2% and the present computations at $Pr = 0.7$ and $Pr = 4$ confirm the negligible dependence of the Nusselt number on the Prandtl number. Indeed, on a much wider Prandtl number range ($4 \leq Pr \leq 1353$) Xia, Lam and Zhou [20] observed a 20% decrease of the Nusselt number in a cylindrical cell of unity aspect ratio and their results were fully confirmed by the Grossmann and Lohse [13] model.

Ahlers and Xu [19] used the prediction by Grossmann and Lohse [12] for $Pr \geq 2$ to fit their data over the range $4 \leq Pr \leq 34$. We have performed a similar fit but, in the present case, we have used the updated and more realistic model by Grossmann and Lohse [13] where the influence of all regions, and not only two, is considered. This theory yields at the same time Nu and Re by

$$\frac{NuRa}{Pr^2} = c_1 \frac{Re^2}{g(\sqrt{Re_c/Re})} + c_2 Re^3, \qquad (1)$$

and

$$Nu = c_3 \sqrt{RePr} \left\{ f\left[\frac{Nu}{2\sqrt{Re_c}} g\left(\sqrt{\frac{Re_c}{Re}} \right) \right] \right\}^{1/2}$$

$$+ c_4 PrRe f\left[\frac{Nu}{2\sqrt{Re_c}} g\left(\sqrt{\frac{Re_c}{Re}} \right) \right].$$

where, it results $f(x) = (1 + x^n)^{-1/n}$ and $g(x) = x(1 + x^n)^{-1/n}$ with $n = 4$ to characterize the 'sharpness' of the transition from one region to another. In (1) the coefficients c_1, c_2, c_3, c_4 and Re_c are to be determined by a non linear fit and, using the data of the three–dimensional numerical simulations with no–slip walls at $Pr = 4$ and $Pr = 0.7$ we have obtained: $c_1 = 92.95$, $c_2 = 0.843$, $c_3 = 0.855$, $c_4 = 0.01364$ and $Re_c = 0.632$. These coefficients have been computed using the same Levenberg–Marquardt method as Grossmann and Lohse [13] and it can be seen from Figure 2 that the agreement with the numerical results is excellent for both values of the Prandtl number. Such a good agreement, however, should not be surprising since the coefficients are obtained from the numerically computed Nusselt numbers; the result of Figure 2b, therefore, should be considered just as a check for the correctness of the fitting procedure. Nevertheless, the second result of the model is the Reynolds number and, since it is not used as input for the calculation of the coefficients c_i and Re_c, this is the real prediction of the theory. The results of Figure 3 show that the prediction of the model is very good, either for the slope of the *Re vs. Ra* curves ($Re \sim Ra^{0.51}$) and for the Prandtl number dependence[1]. Nevertheless we wish to stress that in Figure 3 the

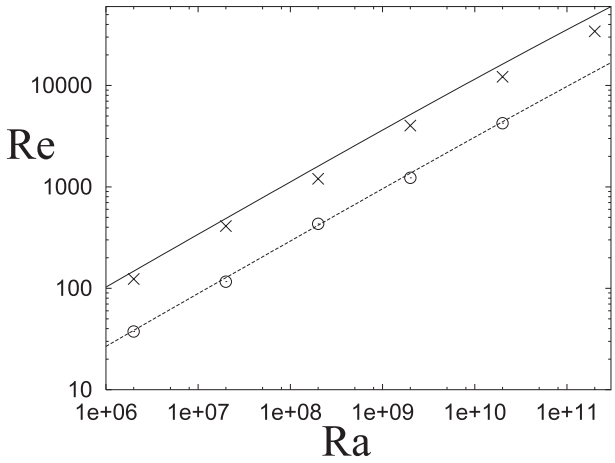

Fig. 3. a) Reynolds *vs.* Rayleigh: × $Pr = 0.7$ (data from VC03); ∘ $Pr = 4$; ——— fit of equation (1) at $Pr = 0.7$; ····· fit of equation (1) at $Pr = 4.0$.

Reynolds number has been computed using the fluctuating velocity u' in the bulk; different values, about 30% bigger but with the same dependence on Ra, would be obtained if the velocity fluctuation were evaluated in the boundary layer regions (see Fig. 14 of VC03). On the other hand, if the Reynolds number were computed using the mean large scale velocity, not only the value but also the dependence on Ra would be missed by the model (see Fig. 12 of VC03). This implies that the prediction of Figure 3 is only a partial success of the model since one of its fundamental ingredients is the presence of a constant wind sweeping the plates; this wind generates laminar viscous boundary layers of the Blasius type at the solid surfaces from which the kinetic energy dissipation rate is estimated. The Reynolds number, therefore, in this context should be defined using the wind velocity U and not the velocity fluctuations u' as in Figure 3.

The essence of the theory by Grossmann and Lohse [12] is to distinguish flow regimes in the Ra–Pr plane depending on the viscous and thermal boundary layer relative thickness and on the dominant contribution (either bulk or boundary layer) to the total kinetic energy ϵ and temperature variance N dissipation rates. We have therefore computed these quantities in order to check if the present simulations are correctly placed in the Grossmann and Lohse Ra–Pr phase diagram (see Fig. 1 of [21]) which, being aspect–ratio dependent has been recomputed for $\Gamma = 1/2$ flows. In Figure 4 we show the boundary layer thicknesses evaluated from the position of the rms peaks of the vertical profiles of temperature and horizontal velocity at $Pr = 4$ (see Fig. 8 of Sect. 3.2); similar results at $Pr = 0.7$ are reported from VC03 for comparison. It can be seen that it results in both cases $\lambda_\theta < \lambda_u$ and λ_θ is essentially the same at $Pr = 0.7$ and $Pr = 4$. In contrast λ_u is always thicker at $Pr = 4$ than at $Pr = 0.7$ owing to the Reynolds number that decreases as the Prandtl number increases. Figure 5 shows the relative contribution of the bulk and the boundary layer regions to the total ϵ and N showing that ϵ is first dominated by the boundary layer

[1] It is worth noting that the fit for the Reynolds number was determined using the rescaling of Grossmann and Lohse [21] who benefitted from more accurate Reynolds number measurements with respect to Grossmann and Lohse [13]; this resulted in a Reynolds number increase by a factor 1.92 (= 0.48/0.25) which considerably improved the prediction.

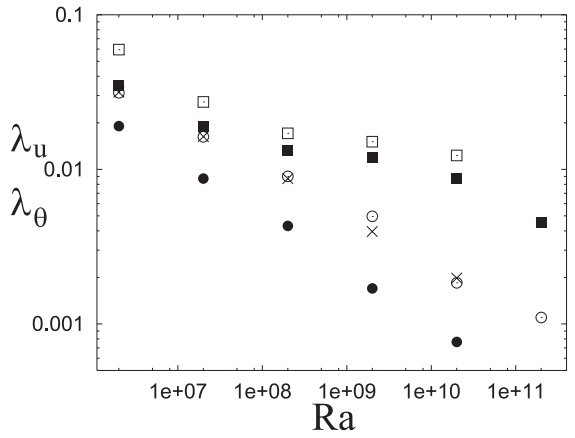

Fig. 4. Boundary layer thicknesses as function of the Rayleigh number: ■ viscous layer, $Pr = 0.7$; ○ thermal layer $Pr = 0.7$; □ viscous layer, $Pr = 4$, × thermal layer $Pr = 4$, ● thermal layer $Pr = 4$ with 'free–slip' boundaries.

and then by the bulk with a transition around $Ra = 10^8$ while N is always dominated by the boundary layer regions. Similar results concerning λ_u and λ_θ were obtained by VC03 at $Pr = 0.7$ with the only difference that the cross–over for ϵ was observed at $Ra \simeq 10^9$. According to the results of Figures 4 and 5 both series of simulations at $Pr = 0.7$ and $Pr = 4$ should be classified as $\mathrm{I_u}$ and $\mathrm{II_u}$ regimes while the Pr and Ra values of the simulations would place them in $\mathrm{I_u}$, $\mathrm{III_u}$ and eventually $\mathrm{IV_u}$ regions (see Fig. 6). We wish to stress that all regions IV pertain to those flows in which the main contribution to the temperature variance dissipation rate N comes from the bulk and they are asymptotic with Ra. In contrast, Figures 4 and 5 suggest that, in this small aspect ratio–cell, the flow eventually goes into the region $\mathrm{II_u}$, which in Figure 6 is absent.

Further analysis is necessary to understand the reason for the mismatch between the good quantitative predictions for Nu and Re of the Grossmann and Lohse [13] model and the 'wrong' positioning of the simulations in the regions of the Ra–Pr phase diagram. Looking at the present results and those of VC03 we can only conjecture that the small value of the aspect–ratio $\Gamma = 1/2$ produces a peculiar evolution of the mean flow which has not been observed in larger aspect–ratio geometries. In fact, the decrease of λ_u with Ra in Figure 4 shows at $Pr = 0.7$ and $Pr = 4$ a 'knee' around $Ra = 10^9$ which VC03 identified as the footprint of the mean flow transition. In particular it was observed that for $Ra \leq 10^9$ the mean flow consisted of axisymmetric toroidal vortices attached to the horizontal plates and a weak recirculation completely filling the cell. At $Ra > 10^9$ the latter structure evolved into two counter–rotating asymmetric unity–aspect–ratio rolls while the toroidal vortices reduced their intensity; this transition was shown to have effects, in addition to the heat transfer, also on the boundary layers dynamics and therefore their contributions to the total kinetic energy and temperature variance dissipation rates.

These results mainly confirm the findings of Roche *et al.* [10] and, keeping in mind the mean flow transition, an interesting result of that paper is the observed bimodality of the Nusselt number in the region $2 \times 10^7 < Ra < 2 \times 10^{10}$. In fact the scatter of the transitional Rayleigh number might be due to the anticipated or delayed onset of the mean flow transition induced by constructive details of the experimental apparatus (finite conductivity and heat capacity of the walls). The horizontality of the cell is another experimental detail that, although special care is taken in the cell positioning, can not be fully ruled out (P. Roche, personal communication).

3.2 Flow with free–slip walls

In the previous section we observed that the viscous boundary layer thickening produced by a Prandtl number increase from $Pr = 0.7$ to $Pr = 4$ neither affects the Nusselt number nor the flow dynamics. The main reason for running the set of numerical experiments with free–slip walls is therefore to prevent the formation of viscous boundary layers and, by comparison with the flows described in the previous section, to analyze the impact of their absence on the flow dynamics. From Figure 2 it is immediately evident that the slope of the Nusselt number *vs.* Rayleigh number and the location of the slope change are the same with and without viscous boundary layers. In other words a model from which the power law is predicted should not depend on the wall velocity profile at least up to $Ra = 2 \times 10^{11}$ and for this small aspect ratio geometry. This suggests that the explanations for the Nu *vs.* Ra power law relying on the velocity distribution inside the boundary layer ([7]) should be ruled out. In fact, Shraiman and Siggia [7] directly relate the Nusselt number to the wall normal velocity gradient $\mathrm{d}u/\mathrm{d}n$ produced by the mean wind through the relation $Nu \sim (\mathrm{d}u/\mathrm{d}n)^{1/3}$. In the present case, however, $\mathrm{d}u/\mathrm{d}n$ is zero owing to the absence of viscous boundary layers and the Nusselt number should also decrease to zero according to the above prediction. In contrast, the results of Figure 2 change in the opposite direction with an increasing Nusselt number for a wall shear stress decreasing to zero. Indeed, an experimental confirmation of this result is given by Solomon and Gollub [22] that artificially enhanced the shear of the bottom boundary layer without changing the Nu behaviour.

Other explanations of the Nu *vs.* Ra relationship based on the boundary layers transition from laminar to turbulent regime ([9]) can not be refuted by the above arguments since this transition occurs beyond $Ra \approx 10^{12}$ ($Ra \geq 10^{14}$ at $Pr = 0.7$ according to [21]) and this is presently out of reach for the direct numerical simulation. Nevertheless if the slope increase of Figure 2 is considered as an indication for the eventual occurrence of the ultimate regime then also the explanations based on the boundary layer transition should be reconsidered since the slope increase is observed also when viscous boundary layers are absent.

The most evident difference between the flows with different velocity boundary conditions is the magnitude of

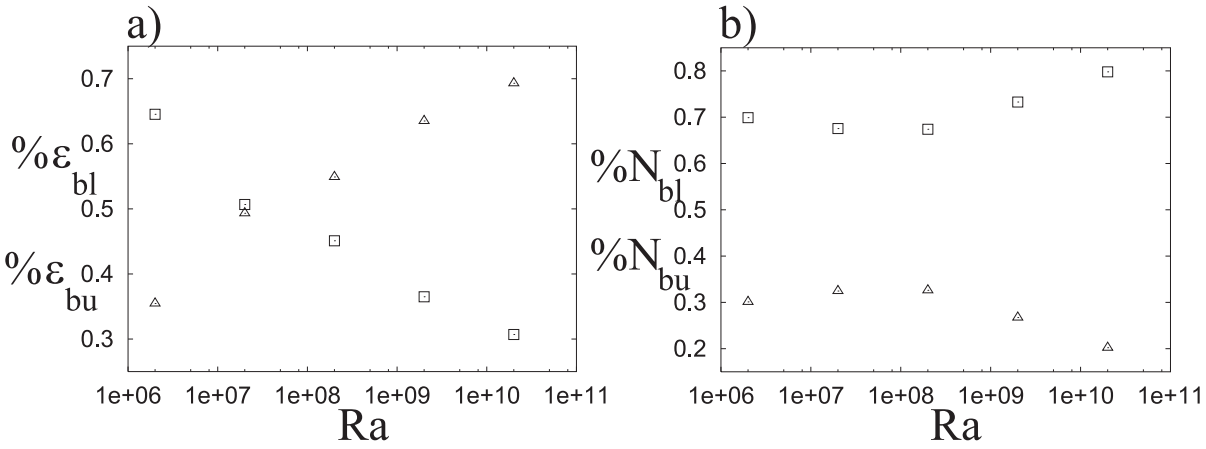

Fig. 5. Percentage of the kinetic energy dissipation a) and temperature variance dissipation rates b) in the bulk and in the boundary layers as function of the Rayleigh number at $Pr = 4$; △ bulk contribution, ◘ boundary layer contribution.

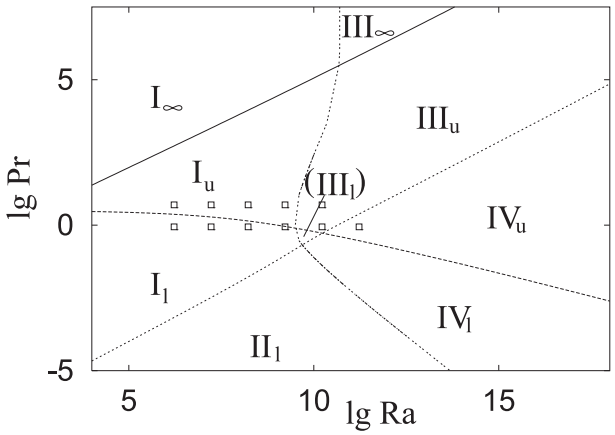

Fig. 6. Grossmann and Lohse phase diagram recomputed for the c_i and Re_c obtained from equation (1) fitted to the present numerical simulations. The ◘ symbols indicate the (Ra, Pr)–coordinates of the numerical simulations.

the Nusselt number that, in the free–slip case, is about twice bigger than in the no–slip case. Looking at Figure 7 it is observed that the flow topology is essentially the same in both cases with the averaged velocities in the free–slip case that only increase by 10–15% with respect to the no–slip case. The peak values of the radial velocity, however, are now located at the plate surfaces where the temperature gradients are the highest; this provides an efficient mechanism for the 'sweeping' of these surfaces from fluid particles which have been heated (or cooled) by pure conduction. The fluctuations of Figure 8, on the other hand, show a dramatic change in the free–slip case, especially for the horizontal velocity in the wall region which increase by a factor in between 2 and 3. The temperature fluctuations also increase and move their peaks closer to the plates were the wind fluctuations are the highest. These phenomena both contribute to increasing the correlation $\langle\theta' u'\rangle$ which is the convective heat transfer.

The mean flow far from the plates also has an active role in the heat transport through the convection of $\langle\theta' u'\rangle$ *via* coherent ascending (descending) hot (cold) currents. In other words, the correlation $\langle\theta' u'\rangle$ drains (delivers) the heat from (to) the hot (cold) plate while the large–scale recirculations, in addition to producing the winds sweeping the plates, behave like flywheels which take care of the transfer between the plates.

Also for the above phenomena Solomon and Gollub [23] have given experimental evidence: in particular they artificially enhanced the strength of the mean recirculation producing an increase of heat transfer up to 50% with respect to the unperturbed value. It should be mentioned, however, that they also observed a decrease in the exponent of the Nu *vs.* Ra power law, even if, owing to the particular experimental technique adopted for the recirculation enhancement, they altered also the mean flow structure.

Before concluding this section we wish to stress that, although by using free–slip surface viscous boundary layers are suppressed, according to Figure 8 still there are strong gradients of horizontal velocity fluctuations at the plates; this implies that some viscous dissipation could yet occur at the plates even if, as shown in Figure 8e, at $Ra = 2 \times 10^{10}$ this secondary contribution becomes comparable to that of the no–slip case.

3.3 Axisymmetric flow

The conclusion of the previous section seems to disagree with the paper by Ciliberto *et al.* [24] that, using vertical screens attached to the horizontal plates, strongly modified the mean flow without noticing appreciable variations of the Nusselt number. In that case, however, the rectangular shape of the cell and the larger aspect ratios ($1 \leq \Gamma \leq 6.5$) did not allow a direct comparison with the present results. In addition, from that paper it was not possible to understand if the mean flow reoriented itself in such a way to flow parallel to the vertical screens and therefore to establish a configuration similar to the unperturbed one. We note, in addition, that a direct comparison of the results of the previous section with

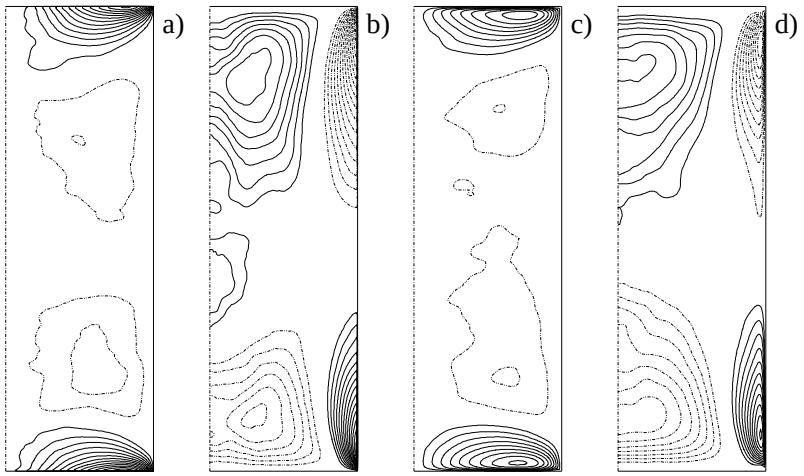

Fig. 7. Mean radial velocity (a) and c)) and vertical velocity (b) and d)) for the flow at $Ra = 2 \times 10^{10}$ and $Pr = 4$. Panels a) and b) are the simulation with free–slip velocity boundary condition, panels c) and d) standard no–slip condition. $\Delta u = \pm 0.04$ ——— for positive ····· for negative values. The data have been averaged over the azimuthal direction and in time.

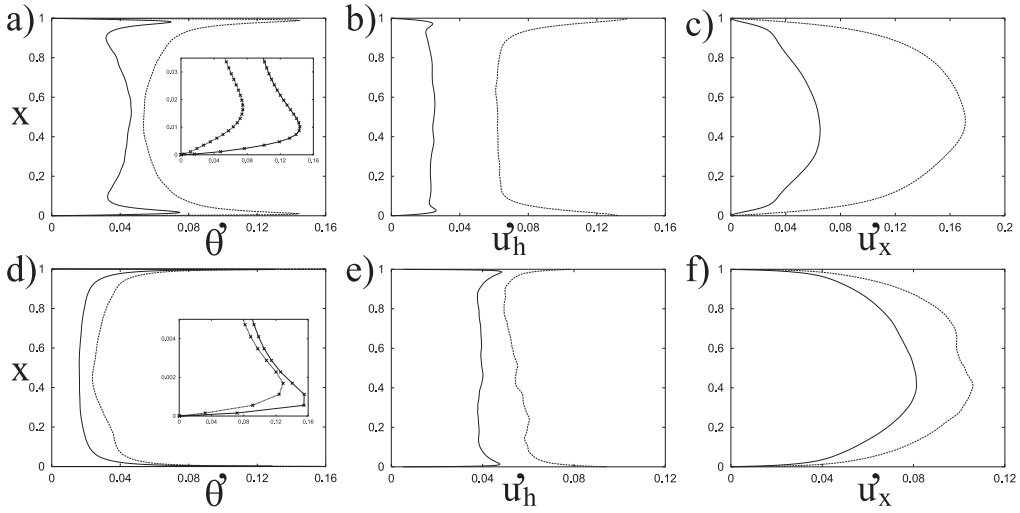

Fig. 8. rms vertical profiles (averaged over azimuthal, radial direction and time) of temperature (a) and d)), horizontal velocity (b) and e)) and vertical velocity (c) and f)); $Pr = 4$, upper panels $Ra = 2 \times 10^7$; lower panels $Ra = 2 \times 10^{10}$. ——— no–slip velocity boundary conditions, – – – – free–slip. The insets in panels a) and d) are zooms of the lower thermal boundary layer region. The symbols on the lines evidence the gridpoint positions.

the paper by Ciliberto *et al.* [24] is not strictly correct owing to the different boundary conditions of the present case which alter, not only the mean flow strength but also the near wall fluctuations. These considerations and the peculiar behaviour of the mean flow never observed in larger aspect–ratio geometries suggested the analysis of a series of axisymmetric simulations with the aim of modifying the mean flow topology and preventing its transition. More in details, in these experiments we have simulated the flow only on a meridional r–x plane thus suppressing the variations in the azimuthal direction and, as a consequence, all the non–axisymmetric large–scale structures. This has a strong impact on the mean flow topology since, as shown in the previous section, it consists of a large scale recirculation which eventually breaks into two counter–rotating rolls; both configurations completely fill the cell and are asymmetric therefore they can not exist in an axisymmetric flow.

The averaged fields are given in Figure 9 where it is observed that, in contrast to the expectations, not only the largest asymmetric mean flow structures but also the toroidal rings attached to the horizontal plates are suppressed by the enforced flow symmetry. The mean large scale flow, in this case consists of a strong ascending current around the symmetry axis and its descending counterpart that only partially sweeps the side wall. As can be seen from Figure 9 for the highest value of the Rayleigh number additional smaller structures appear even if the basic features of the mean flow remain unchanged. In particular the upward hot current around the axis and the wind direction on the horizontal plates (radially outward for the upper plate and mixed inward/outward for

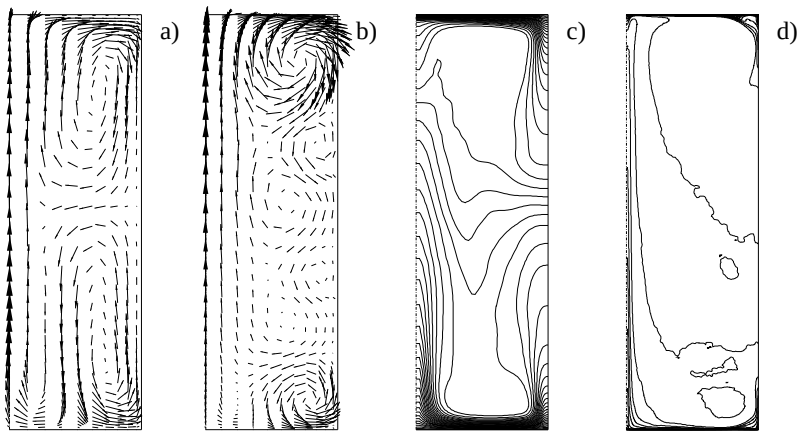

Fig. 9. Mean velocity vectors (a) and b)) and temperature (c) and d)) for the axisymmetric flow at $Pr = 4$. Panels a) and c) are at $Ra = 2 \times 10^7$, panels b) and d) at $Ra = 2 \times 10^{11}$. $\Delta\theta = 0.02$. The data have been averaged only in time.

the lower plate) remain the same over the whole range of Rayleigh numbers without evidence of the transition that in the three–dimensional flow occurred around $Ra = 10^{10}$. The heat transfer curve of Figure 2 confirms the absence of flow transition since, apart from the first point at $Ra = 2 \times 10^6$ where the flow was multi–periodic in time and therefore not well developed yet, only a single power law is observed with $Nu \sim Ra^{0.3}$.

It might be objected that this last result is an artifact of the imposed symmetry since it alters not only the large scales but also the plume and boundary layer dynamics that in a full three–dimensional flow is considerably different from an axisymmetric one. We note, however, that the severe changes of the wall dynamics produced by the free–slip boundary conditions did not affect neither the slope of the Nu *vs.* Ra relation nor its change around $Ra \simeq 10^9$, it is therefore plausible that the single slope observed in the axisymmetric flow is an effect of its mean flow.

For the sake of completeness we wish to mention the work by Umeura and Busse [25] that investigated, by an asymptotic analysis and imposing free–slip velocity boundary conditions, the axisymmetric convection at large Rayleigh and infinite Prandtl number; although they were seeking for steady solutions, in agreement with Figure 9, they found that the flow develops a central plume and a peripheral current with different features. They also pointed out that, if fluid physical properties are assumed to be independent of the temperature, the solutions having an ascending or descending central plume are both possible while, when material properties are temperature dependent, one of the two solutions will be preferred in general.

4 Closing remarks

We have performed a series of numerical experiments with the aim of investigating the effects of the mean flow and viscous boundary layers on the flow dynamics in thermal convection. In a first series of runs we have increased the Prandtl number from $Pr = 0.7$ to 4; this has produced a substantial increase of the viscous boundary layer thickness while leaving unchanged the thickness of the thermal layers and therefore the non dimensional heat transfer. A second set of experiments was run at $Pr = 4$ but with free–slip velocity boundary conditions thus avoiding the formation of viscous boundary layers. These experiments indicated that the absence of viscous boundary layers only alters the magnitude of the Nusselt number leaving unchanged the power law dependence on the Rayleigh number and the slope increase starting around $Ra \simeq 10^9$. This confirmed the idea proposed in VC03 that the heat transfer transition is induced by a change of the mean flow structure which is initially dominated by toroidal axisymmetric structures attached to the plates and eventually by two counter–rotating asymmetric unity–aspect–ratio recirculations. This suggested a third set of experiments with the flow artificially maintained axisymmetric with the aim of changing the large–scale flow and suppressing its transition. We have observed in this case a different structure of the averaged flow whose topology remained essentially the same in the range $2 \times 10^6 \leq Ra \leq 2 \times 10^{11}$; accordingly the Nusselt number followed a unique power law with Rayleigh number which to a good approximation is $Nu \sim Ra^{0.3}$.

To summarize, the results indicate that the presence of the viscous boundary layers has little or negligible influence on the *slope* of the Nu *vs.* Ra relation. The boundary layers have, instead, a big effect on the intensity of the velocity and temperature fluctuations and on the strength of the recirculations both affecting the *magnitude* of the Nusselt number.

We wish to stress that the above conclusions have been drawn from simulations performed in a $\Gamma = 1/2$ aspect–ratio cylindrical cell and they should not be extended to larger aspect–ratio geometries without further analysis. It has been shown (VC03), in fact, that the $\Gamma = 1/2$ cell yields a mean flow dynamics which has not been observed for larger values of Γ and this might the reason for the peculiar behaviour of the present flow.

The author is indebted to Prof. D. Lohse for fruitful discussions, for his comments on a preliminary version of this manuscript and for providing the code for the Levenberg–Marquardt non linear fit of equation (1) to the numerical data. The author has benefitted form several discussions with Prof. R. Camussi. The paper was prepared with the financial support of CEMeC of Politecnico di Bari. Drs. F. Massaioli and G. Amati from CASPUR (Consorzio interuniversitario per le Applicazioni di Supercalcolo Per Università e Ricerca) are gratefully acknowledged for the technical support in implementing openMP and using parallel computers.

References

1. G. Ahlers , Phys. Rev. E **63**, 015303 (2001)
2. P.E. Roche, B. Castaing, B. Chabaud, B. Hebral, J. Sommeria, Eur. Phys. J. B **24**, 405 (2001)
3. J.J. Niemela, K.R. Sreenivasan, J. Fluid Mech. **481**, 355 (2003)
4. R. Verzicco, J. Fluid Mech. **473**, 201 (2002)
5. S. Chaumat, B. Castaing, F. Chillà, *Rayleigh–Bénard cells: influence of the plate properties Advances in Turbulence IX*, edited by I.P. Castro, P.E. Hancock, id:46,1 (CIMNE, Barcellona 2002)
6. B. Castaing, G. Gunaratne, F. Heslot, L. Kadanoff., A. Libchaber, S. Thomae, X.Z. Wu, S. Zaleski, G. Zanetti, J. Fluid Mech. **204**, 1 (1989)
7. B.I. Shraiman, E.D. Siggia, Phys. Rev. A **42**, 3650 (1990)
8. X. Chavanne, F. Chillà, B. Castaing, B. Hébral, B. Chabaud, J. Chaussy, Phys. Rev. Lett. **79**, 3648 (1997)
9. X. Chavanne, F. Chillà, B. Chabaud, B. Castaing, B. Hebral, Phys. Fluids **13**, 1300 (2001)
10. P.E. Roche, B. Castaing, B. Chabaud, B. Hebral, Europhys. Lett. E **58**, 693 (2002)
11. R. H. Kraichnan, Phys. Fluids **5**, 1374 (1962)
12. S. Grossmann, D. Lohse, J. Fluid Mech. **407**, 27 (2000)
13. S. Grossmann, D. Lohse Phys. Rev. Lett. **86**, 3316 (2001)
14. R. Verzicco, R. Camussi, J. Fluid Mech. **477**, 19 (2003)
15. X.Z. Wu, *Along a Road to Developed Turbulence: Free Thermal Convection in Low Temperature Helium Gas*, *Ph.D. thesis*, University of Chicago (1991)
16. J.J. Niemela, L. Skrbek., R.R. Sreenivasan, R.J. Donnely, Nature **404**, 837 (2000)
17. P.E. Roche, B. Castaing, B. Chabaud, B. Hebral, Phys. Rev. E **63**, 045303-1–045303-4 (2001b)
18. G. Grötzbach, J. Comput. Phys. **49**, 241 (1983)
19. G. Ahlers, X. Xu, Phys. Rev. Lett. **86**, 3320 (2001)
20. K.Q. Xia, S. Lam, S.Q. Zhou, Phys. Rev. Lett. **88**(6), 064501-1–4 (2002)
21. S. Grossmann, D. Lohse, Phys. Rev. E **66**, 016305-1 – 016305-6 (2002)
22. T.H. Solomon, J.P. Gollub, Phys. Rev. Lett. **64**, 2382 (1990)
23. T.H. Solomon, J.P. Gollub, Phys. Rev. A **43**, 6683 (1991)
24. S. Ciliberto, S. Cioni, C. Laroche, Phys. Rev. E **54**, 5901 (1996)
25. A. Umeura, F. Busse J. Fluid Mech. **208**, 459 (1989)